# Chapter 2 Literature reviews

## 2.1                                                                     CNTs and their features

Since CNTs were first discovered and reported by Dr. Iijima in 1991, it has been researched for more than 10 years. CNTs can be considered the "elongated" fullerene, as Fig. 2-1 shown [Dresselhaus 96-756]. Dr. Iijima envisaged CNTs comprises coaxial cylinders of closed graphitic sheets composed of carbon hexagon (Fig. 2-2 (a)), separated by a distance about 0.34 nm, and its both sides are seamless [Iijima, 91-56]. Furthermore, a helical arrangement of carbon hexagons was also observed by Dr. Iijima (Fig. 2-2 (b)). Depend on the number of graphitic sheets, CNTs can be generally divided into single-walled CNTs (SWNTs) and multi-walled CNTs (MWNTs).

CNTs are treated as 1-D structure and they mainly consist of $sp^2$ C-C bonds. In mathematics, they can be characterized by a pair of integers (n, m) to describe the structural orientation. Furthermore, chiral vector is defined as $C_h = na_1 + ma_2$ (Figs. 2-3 (a), (b) [Saito 92-2204]), and the included angle between $C_h$ and $a_1$ is defined as chiral angle (θ). For comparison, depend on the different orientation of rolling axis, the (n, n) type CNTs has a chiral angle θ = 30$^o$ called armchair form [Fig. 2-1 (a)]; the (n, 0) type and (0, m) type CNTs have a chiral angle θ = 0$^o$ called zigzag form [Fig. 2-1 (b)]; the (n, m) type CNTs have a chiral angle ranging from 0$^o$ to 30$^o$ called chiral form [Fig. 2-1 (c)]. The phenomena that chiral vector can influence CNTs electronic structure has been proved by Saito and coworkers, the results are summarized as follows [Saito 92-2204]:

(1) When n - m = 0, the CNTs have metallic property (armchair form).

(2) When n - m = 3q, the CNTs are small band semiconductor ($E_g \sim$ 1.7-2.0 eV).

(3) When n - m $\neq$ 3q, the CNTs are semiconducting ($E_g \sim$ 0.5-0.6 eV).

As for the CNTs morphologies, for example, bamboo-like CNTs [Lee 00-3397], Y-CNTs CNTs [Li 01-1879], helical-like CNTs [郭 04-P. 4-24], H-junction CNTs [Ting 02-324], and bill-like CNTs [郭 04-P. 4-25], et al. were observed (Figs. 2-4 (a) ~ (e), respectively). The morphologies of CNTs are determined by the used apparatus (arc-discharge, laser ablation, CVD, et al) and applied parameters (catalyst, temperature, precursor, et al.). Furthermore, the features and properties of CNTs can be changed via some post-treatment steps, as described in later graphs.

## 2.2 Nanofabrications of the open-ended CNTs

CNTs tips were opened for the sakes of increasing field emission current, capping CNTs with material, benefiting hydrogen adsorption properties, etc. So far several methods of fabricating the open-ended CNTs have been proposed. Nevertheless, most of these methods suffered from the drawback of not-good performing reproduction or causing serious structure damage to CNTs. Our proposing post-treatment comprises H-plasma etching and chemical etching can apparently increase the possibility of producing well structure and undestroyed open-ended CNTs. The recent reports about fabrications of open-ended CNTs are described later.

### 2.2.1 Oxidation method

The group of Kung has reported a process that put CNTs sample in an oven at $400^{\circ}C$ for a period of time in the presence of $O_2$. The TEM images of CNTs treated by $O_2$ oxidation for 20 min at 400 °C is shown in Fig. 2-5. The results show a lot of CNTs tips were opened or partially opened. It is suggested owing to the different strained stress at the tip and side wall of CNTs, the highly strained CNTs end tips will be first oxidized

by $O_2$ than the less strained side walls of CNTs [Kung 02-4819].

## 2.2.2  Plasma etching methods

(a) Tsai's group reported a method to open CNTs caps by H-plasma etching. First, the Pd-assisted aligned CNTs were fabricated by MPE-CVD system. Then, CNTs were etched by high concentration H-plasma. The substrate was enhanced high negative bias, and therefore the positive ions in H-plasma would bombard the substrate. The CNTs tips will be removed by the H-plasma etching. Moreover, the negative bias would cause a strong local bias current, and it heated the aligned CNTs and resulted in the melt of Pd particles. After that, the molten Pd particles were drawn into the opened-tips and elongate to form Pd nanorods (Fig. 2-6). The Schematic of the growth mechanism is shown in Fig. 2-7 [Tsai 99-3462].

(b) Chung and coworkers fabricated base-growth CNTs by PECVD system. They used 70 nm Co-Ni film as catalyst and the CNTs were deposited using $CH_4$ and $H_2$ mixture at a pressure of 20 mtorr. The close-ended CNTs tip structure is shown in Fig. 2-8 (a).

After CNTs deposition, $CF_4$ plasma was chosen to etch the CNTs film. The authors detected amorphous carbon and graphite particles are more easily etched than CNTs by $CF_4$ plasma. Thus the unwanted carbonaceous materials such as amorphous carbon and graphite particle could be selectively removed before the destruction of CNTs structure. Then, the CNTs with open-ended tip structure were generated as indicated in Fig. 2-8 (b) [Chung 01-73].

**(c)** Lee, et al. proposed a process to fabricate open-ended CNTs in application of hydrogen storage. Curly and close-ended MWNTs were fabricated by Microwave Plasma Enhanced Chemical Vapor Deposition (MPE-CVD) with $H_2$ (99.9%, vol %) and $CH_4$ (0.1%). The microwave power, working pressure, temperature are 700 W, 30 Torr and 750℃.

Furthermore, they found aligned and open-ended CNTs could be obtained by addition of few oxygen content in the mixed source gas comprised $H_2$: 89.9 vol%, $CH_4$: 0.1 vol% and $O_2$: 10 vol%. The tubes were mostly opened owing to the oxygen plasma etching effect as shown in Fig. 2-9 [Lee 02-577].

**(d)** The CNTs were fabricated via pyrolysis of metal-containing organometallic precursor. As Fig. 2-10 (a) shown, the as-grown CNTs film was occasionally covered with a thin amorphous carbon layer (0.1~0.5μm). Huang and his coworkers adopted radio frequency glow-discharge $H_2O$ plasma with relatively mild intensity to etch the amorphous carbon layer coated on CNTs tips (Fig. 2-10 (b)), and thus tip catalyst particles were directly exposed to environment. Afterwards the CNTs sample was gently washed with HCl (37%), and then the Fe catalyst particles were dissolved and in result of open-ended CNTs as Fig. 2-11 shown [Huang 02-3543].

## 2.2.3　Chemical etching methods

**(a)** Group of Wang fabricated CNTs by bias-enhanced MP-CVD system, and Stainless 304, Ni, and Co were used as catalysts [Wang 01-4028]. $CH_4$ and $H_2$ were then mixed in the chamber. The flow rates of these two precursors were 20 sccm and 80 sccm respectively.

The working pressure is about 1.2 Torr and a 180 V negative bias was applied to the substrate. The temperature of the substrate was estimated to about 500 ~ 600°C because of the plasma energy.

After CNTs growth [Fig. 2-12 (a)], the CNTs substrate was electrochemical etched in a solution with a D.C. voltage of 1.5 V, and then the metal particle was immediately removed without damaging CNTs structure. Then, the open-ended CNTs were obtained as displayed in Fig. 2-12 (b).

**(b)** It was proposed by Tsang's group that CNTs tips can be opened by nitric acid treatment. In the first place, the close-ended CNTs were prepared by arc vaporization. Then, the close-ended CNTs samples were suspended in condensed nitric acid, and followed by their standard heat treatment processes. The results indicate the CNTs tips are opened. And it also shows CNTs are attacked particularly at the external or internal curved regions which may be composed of five-membered carbon ring (arrows mark the external curved areas in Figs. 2-13 (a) and internal curved regions in (b) and (c)) [Tsang 94-159].

## 2.2.4   AAO template-assisted and Ar+ ion milling method

Yoon's group has proposed a method to fabricate the open-ended CNTs as noted later [Yoon 04-825]. First, ordered AAO template was prepared through the two-step anodization process, and then the CNTs include no catalyst and bamboo-like structure were deposited into the AAO template by a tube furnace with a mixture source gas containing acetylene (5%) and nitrogen (100 sccm) at 550°C for 50 min. The schematic processes of fabricating the close and open tip of CNTs are shown in Fig. 2-14. If the

bottom side of specimen was slightly ion milled by $Ar^+$ bombardment and then immersed in acid solution, which can only etch off AAO template (CNTs will not be removed owing to their high chemical stability), thus the close-ended CNTs were generated [Figs. 2-14 (a) → (b) → (d)]. On the other hand, when the bottom side of specimen suffered $Ar^+$ bombardment with relative higher intensity, and the specimen was subsequently etched in acid solution in result of open-ended CNTs [Figs. 2-14 (a) → (c) → (d)]. The close-ended and open-ended CNTs are shown in Figs. 2-15 (a) and (b), respectively. The height of CNTs could be determined by changing the etching time in acid solution [Yoon 04-825].

## **2.3        Properties and potentialities of open-ended CNTs**

Because CNTs are composed of graphitic sheets, therefore, they have lots of superior intrinsic characteristics with respect to graphite, e.g. good thermal stability, stable chemical inert, high conductivity, and excellent mechanical strength, et al. Moreover, CNTs have ultra-high aspect ratio and low workfunction, which facilitate the tunneling effect. These extraordinary physical and chemical properties and their potentialities are noted as follows:

**(a) Field emission**

Field emission behavior involves the extraction of electrons from a bulk surface by tunneling effect through the potential barrier in surface. The emitted current is determined by the local electric field (E), and the workfunction ($\phi$) of the electric emitter. For extraction of electron, the local field needs to go up to 2-3 V/nm, hence the

emitter should have a sharp tip to bring about the field amplification effect, i.e. the electric field lines are concentrated around the tip with high aspect ratio. It have been proved CNTs own several particular properties include low work function, ultrahigh aspect ratio, high chemical and thermal stability, and therefore it is the proper candidate to be utilized for flat panel displays, backlights for liquid crystal displays, cathode ray tubes, traffic signals. Furthermore, it is found the open-ended CNTs have ultra-high aspect ratio of tips and it can lead to a raise of emission current. Thus, open-ended CNTs can be used to enhance field emission performance in the application of field emitter.

## (b) Hydrogen storage

Hydrogen storage technique of CNTs was come from the concept of high specific area of CNTs. Rodriguez and Baker speculated hydrogen can be stored up to 75 wt % in a carbon nano-fiber cartridge. Depend on their claim, it is inferred one carbon can store nine hydrogen atoms [Kuo 03-P. 27].

It has been reported open-ended CNTs perform higher hydrogen storage capacity than close-ended CNTs by Lee's group [Lee 02-577]. It is considered open-ended CNTs possess higher specific surface area than close-ended CNTs due to the extended surfaces in the hollow cavities. It was speculated the inner cavity of CNTs could be the major site of hydrogen storage, and the high temperature storage site is in connection with adsorption in defective regions. For hydrogen storage in open-ended CNTs, they further concluded the chief hydrogen storage mechanism at ambient temperature is hydrogen physisorption in the hollow cavities. However, the irreversible chemisorbed hydrogen is ascribed to the formation of C-H bonds in the defective regions through hydrocarbon decomposition.

## 2.4　　　　　　　　Nanofabrications of the material-filled CNTs

### 2.4.1　Material filling during CNTs deposition

To realize nano-resolution perpendicular recording media, Kuo's group successfully used magnetic material as catalyst to synthesize magnetic metal-encapsulated CNTs by ECR-CVD with $CH_4$ and $H_2$ as source gases. The catalyst nanoparticles were naturally encapsulated to CNTs tips during CNTs deposition. Five different magnetic materials such as Fe–Pt, Co–Pt, $Nd_2Fe_{14}B$, Fe and Fe–Ni, were adopted to be catalyst for CNTs deposition. According to the authors' experimental observations, they found all CNTs were vertically aligned and tip-growth, the maximum tube number density went up to 134 $Gtubes/inch^2$.

From AFM and the corresponding MFM images [Fig. 2-16], the nanoparticles were well-distributed, and the signal spots, i.e. magnetic field of each CNTs tip nanoparticles could be detected and read. Their results proved the promising applications in magnetic recording media by means of magnetic metal-encapsulated carbon nanostructures [Kuo 03-799].

### 2.4.2　Material filling after CNTs formation

It has been reported recently that CNTs can be filled with materials to be utilized as nano-template or nano-composite. Filling techniques contain physical and chemistry methods depend on the surface tension of molten materials as noted later.

(a) Physical filling methods:

For filling CNTs with material, CNTs caps need to be opened and a surface tension

of less than 100~200mNm$^{-1}$ is necessary for molten material to wet and fill hollow cavities of CNTs through capillary action [Ajayan 95-564]. Several molten materials with low surface tension such as Pb, $V_2O_5$, and $AgNO_3$, et al. have been reported for filling CNTs.

Take Pb filling for example, Ajayan and coworkers heated the close-ended CNTs in air with lead. It was found only 1% CNTs tips were opened and filled with lead. The reason should be related to the low yield percentage of open-ended. In addition, Ajayan, et al. suggested a series of physical methods for filling CNTs with $V_2O_5$ [Ajayan 95-564], i.e. CNTs were oxidized in air to open their tips first, and then the partially opened CNTs were mixed with pure $V_2O_5$ powder (has an exceedingly low surface tension about 80 mNm$^{-1}$) and subsequently heated to a temperature greater than the melting point of the oxide in air for a period of time. A large fraction of open-ended CNTs were filled with the oxide as shown in Fig. 2-17. The results depict some fillings display a preferred orientation relationship with the tube axis, and the cavity size determines the crystallization degree of filling (cavity size smaller than 3 nm can result in the formation of amorphous filling).

In addition, a physical filling method has been mentioned in above paragraph, the preparation of open-ended CNTs was carried out via plasma and chemical etching (Fig. 2-12). Huang, et al. further immersed the open-ended CNTs in $AgNO_3/CH_3COCH_3$ solution for 24 hour under magnetic stirring. Then, the samples were heated at 300 ℃ for 2 hour. As shown in Fig. 2-18, open-ended CNTs were filled with the Ag nanorods owing to the decomposition of $AgNO_3$ which was drawn into the hollow channels [Huang 02-3543].

(b) Chemical filling methods:

Tsang, et al., proposed a chemical filling method which is suitable for filling CNTs. Fabrication of filled CNTs was carried out by soaking close-ended CNTs in nitric acid solution containing nickel nitrite, after that, followed by their standard heat treatment.

The TEM image of filled CNTs is represented in Fig 2-19 The results show the CNTs are selectively attacked at the regions with greatest curvature, therefore, 80 % of CNTs were opened by nitric acid treatment, and 60~70 % open-ended CNTs contained Ni material. It was speculated the nickel nitrite solution was sucked into the cavities as the tips were opened [Tsang 94-159].

## 2.5    Storage mechanisms of optical phase-change storage media

From then on, high density rewritable optical data storage receives great attention. So far, the most popular phase-change recording materials contain two categories, Ge-Sb-Te and AgInTe, which are listed in Table 2-1. The optical storage density is restricted by the diffraction limit of the laser beam. However, with the development of short wave-length laser, the storage density can be greatly increased. A focused short wave-length laser beam was used as heat source to irradiate micron-size areas on the chalcogenide film. It was found that the local irradiated regions can be reversely transformed between amorphous and crystalline state. The different optical properties between these two states should be large enough to be utilized for digital data storage application. In order to write a bit, for example, the crystalline location should be molten by laser irradiation with relative higher intensity and then quenched into amorphous phase. The cooling rate has to be greater than the critical cooling rate of amorphizing to prevent recrystallization. On the other hand, for the intention to erase a bit, amorphous regions should be heated above the glass transition temperature by laser irradiation with proper intensity for enough time, which can facilitate the happening of recrystallization. [Frendrich 01-239]. For reading data, the recording spot is irradiated by a weaker laser beam to avoid the undesired phase transformation. It can carry out the purpose to distinguish the

digital signals such as "1" and "0" by detecting the intensity of reflected light. A high reflectivity contrast C is required, which is defined as:

$$C = 2 (R_f - R_i) / (R_f + R_i)$$

Where $R_i$ and $R_f$ are the reflectivity of the regions before writing and after writing, respectively [Men 98-21]. The C value has to reach a detectable range; otherwise the amorphous and crystalline states can't be distinguished by their different reflectively.

## 2.6　　　Specifications of the typical rewritable memory media

There are three stoichiometric compositions of $GeSb_4Te_7$, $GeSb_2Te_4$, and $Ge_2Sb_2Te_5$, in the $GeTe-Sb_2Te_3$ psedobinary system, as illustrated in Fig. 2-20 [Yamada 91-2849]. Some basic physical and chemical properties of the three elements, Ge, Sb, and Te, are compiled and shown in Table 2-2. It has been reported the materials with composition centering around the $GeTe-Sb_2Te_3$ psedobinary system have the following reported properties for rewritable memory media [Kooi 02-3584; Yamada 91-2849]:

(a) Have a large reflectivity contrast between amorphous and crystalline state.

(b) Small volume change between amorphous and crystalline state.

(c) Fast crystallization rate.

(d) Having proper thermal conductivity.

(e) A sufficient number of overwrite cycles (more than $10^5$ cycles).

(f) High carrier-to-noise ratio to enhance the detectable ability.

(g) High thermal stability at room temperature (at least stable for more than 30 year).

(h) Phase change properties can be precisely controlled within a wide range of selected

composition.

## 2.7                                                               Analysis methods

### 2.7.1 Analyses of CNTs

CNTs are usually synthesized in the diameter below several hundred nanometer and length are μm level. Scanning electron microscopy (SEM) is the most convenient and efficient tool to show the surface morphology of CNTs owing to its high magnification (~ 500 K) [郭 04-P. 5-34]. Furthermore, transmission electron microscopy (TEM) is presently a powerful tool for users being able to observe the microstructure of CNTs in depth [郭 04-P. 5-37]. The main advantage of TEM analyses is related to its high resolution for examining the nano-structure of individual tube. As for high resolution transmission electron microscopy (HRTEM) [郭 04-P. 5-38], it provides an effective way to determine the number of graphite layers and the distance of graphite-graphite layers of CNTs. By Raman spectroscopy, two obvious peaks at 1350, 1580 cm$^{-1}$ are defined as D-band and G-band, respectively. The relative intensity ratios of $I_D/I_G$ are used to determine the graphitization degree of CNTs. The graphitization degree decreases with the raise of $I_D/I_G$ ratio[郭 04-P. 5-51].

### 2.7.2   Analysis methods of phase-change storage media

For optical change observations, static tester can be used to examine the relative

reflectivity contrast between amorphous and crystalline states. The analysis method of static tester is simultaneously writing and erasing at the same spots on the samples (samples are heated). The temperature where the transmissivity abruptly changes is defined as the transition temperature. It can also measure the sensitivity, transition time, activation energy of crystallization, endurable overwrite cycles, and reflectivity contrast, during amorphous-to-crystalline or crystalline-to-amorphous transformations.

Differential scanning calorimetry (DSC) is another method to measure the transition temperature. The appreciable amount of powder sample is heated with a proper heating rate. A Kissinger's plot is created to examine the activation energies of crystallization. For example, DSC curves for the GeTe-Sb$_2$Te$_3$ psedobinary system is shown in Fig. 2-21 [Yamada 91-2849].

Table 2-1 List of phase-change material [王, 98-P. 121].

| Type of phase change | Materials |
|---|---|
| Amorphous → crystalline (irreversible) | Te-TeO$_2$, Te-TeO$_2$-Pd (CD-R) Sb$_2$Se$_3$/Bi$_2$Te$_3$ |
| Amorphous ←→ crystalline (reversible) | Ge-S-Sb-Te Ge-Sn-Te-TeO$_2$ Ge-Sn-Te Se-Sn-Te Sb-Se, Sb-Se-Te Ga-Se-Te, Ga-Ge-Se-Te Ge-Sb-Te (DVD-RAM) In-Se-Te, Ag-In-Sb-Te (CD-RW) |
| Crystalline ←→ crystalline | Ag-Zn Cu-Al-Ni In-Sb, In-Sb-Se, In-Sb-Te |

Table 2-2 Basic physical properties of Ge, Sb, Te and Co [http://environmentalchemistry].

| Element | Ge | Sb | Te | Co |
|---|---|---|---|---|
| Atomic number | 32 | 51 | 52 | 27 |
| Atomic radius (A) | 1.52 | 1.53 | 1.42 | 1.67 |
| Atomic volume (cm$^3$/mol) | 13.6 | 18.23 | 20.5 | 6.7 |
| Crystal structure | FCC | Rhombohedral | Hexagonal | Hexagonal |
| Electron work function (eV) | 5 | 4.55 | 4.95 | 5 |
| Melting point (℃) | 937.4 | 630.9 | 449.65 | 1495 |
| Heat of vaporization (kJ/mole) | 330 | 77.14 | 52.55 | 376.5 |
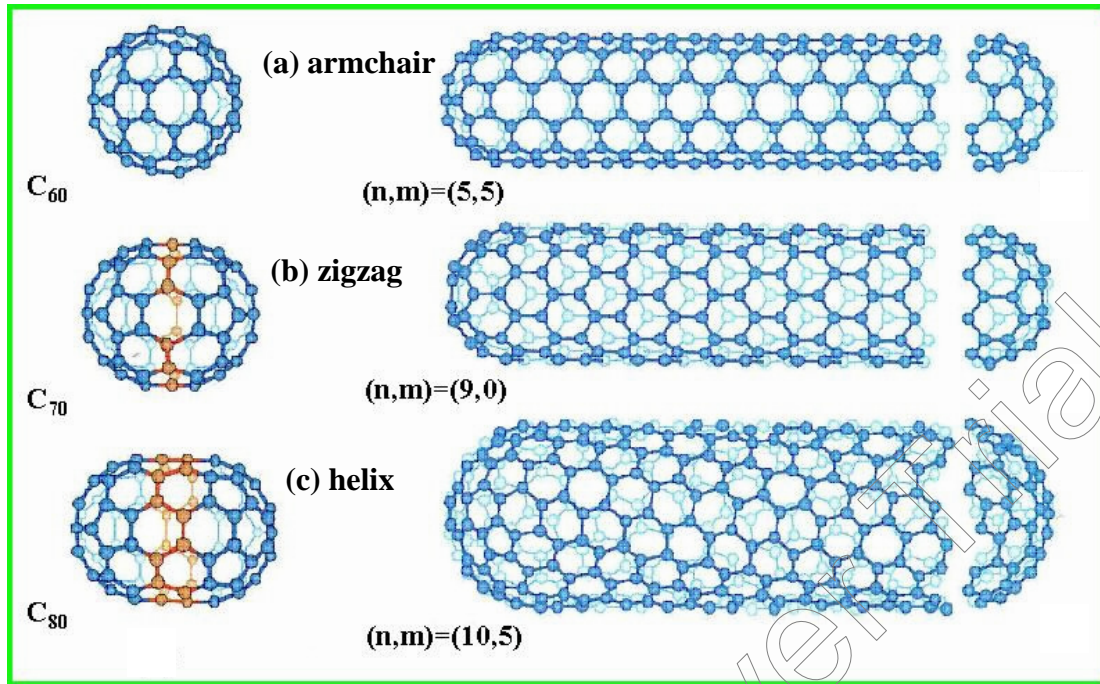
Fig. 2-1 Depiction of fullerene and CNTs structure. CNTs can be considered the "elongated" fullerene [Dresselhaus 96-P. 756].
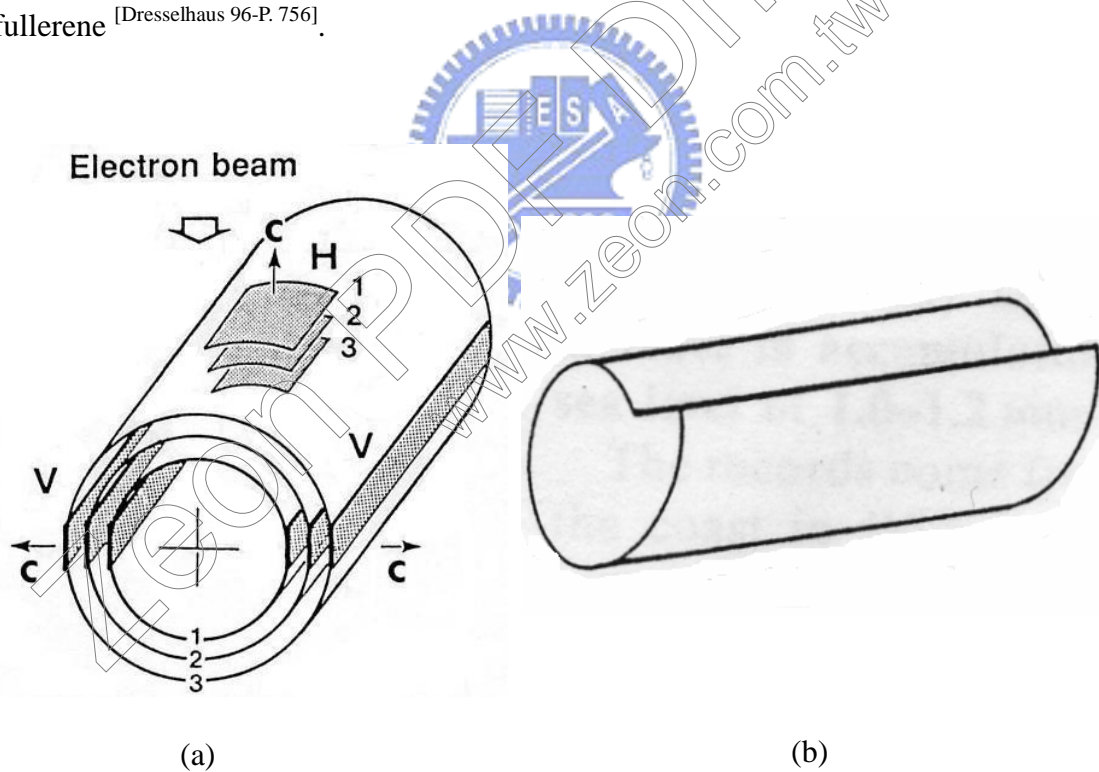


Figs. 2-2 The possible structure models of a graphitic tubule (a) Each cylinder represents a coaxial closed layer of carbon hexagons. (b) Helical arrangement of carbon hexagons [Iijima 91-56].
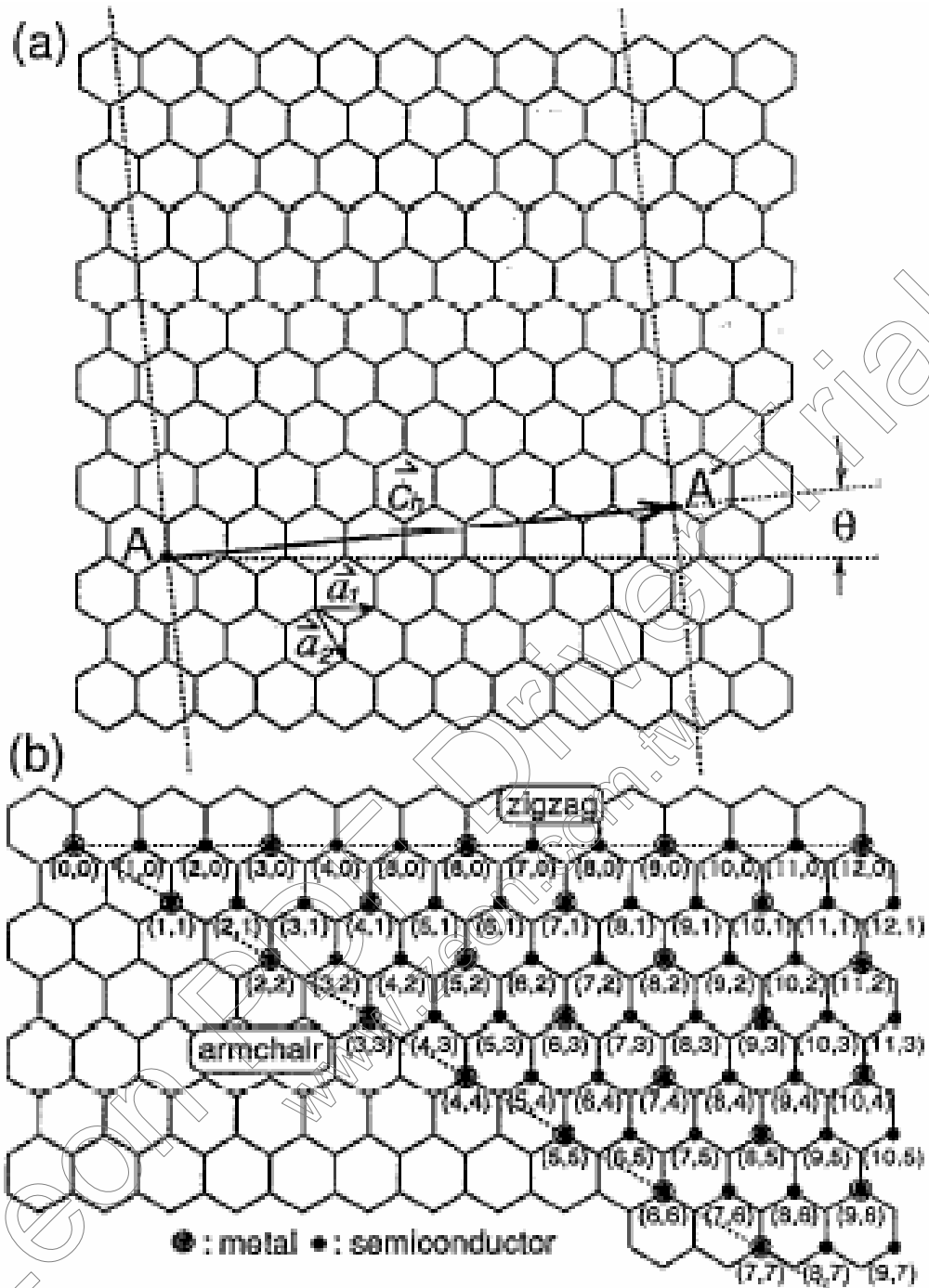
Figs. 2-3 (a) Graphene tubules are made by rolling a graphene sheet into a cylinder. The tubules are uniquely determined by their lattice vectors ck The chiral angle is denoted by 8, while a, and a, denote the unit vectors of graphite. (b) Possible vectors for chiral fibers. The circled dots and dots, respectively, denote metallic and semiconducting behavior for each Fiber [Saito 92-2204].
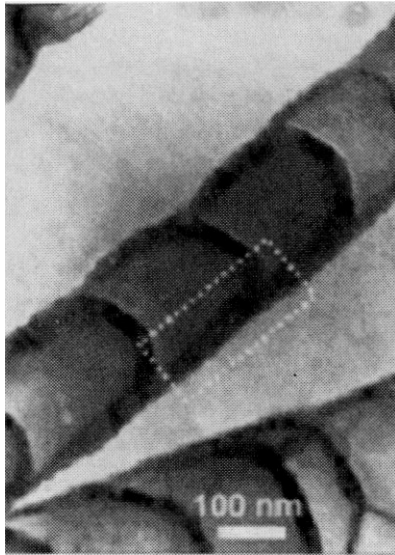
(a)
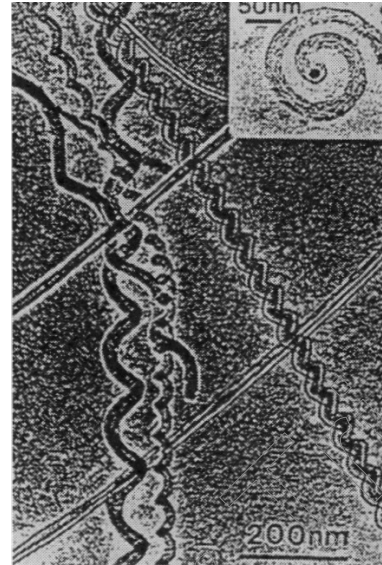
(b)
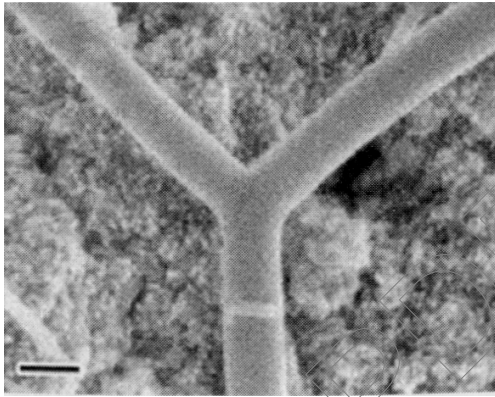
(c)
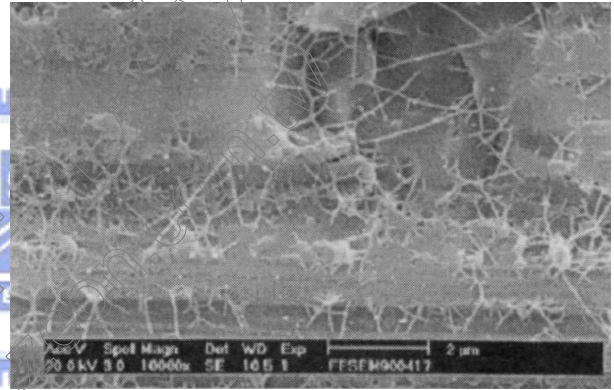
(d)
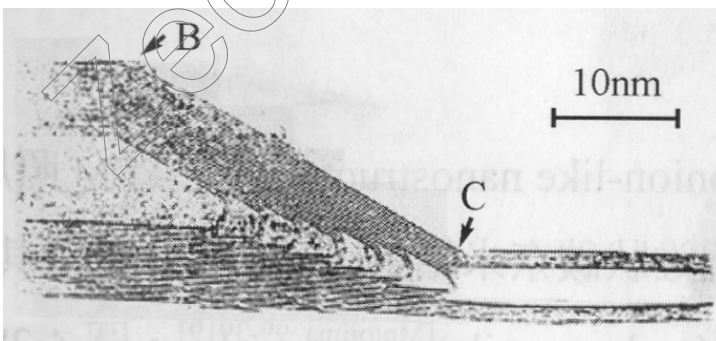
(e)

Figs. 2-4 (a) Bamboo-like CNTs [Lee 00-3397]. (b) Y-junction CNTs [Li 01-1879]. (c) Helical CNTs [郭 04-P. 4-24]. (d) H-junction CNTs [Ting 02-324] (e) Bill-like CNTs [郭 04-P. 4-25].
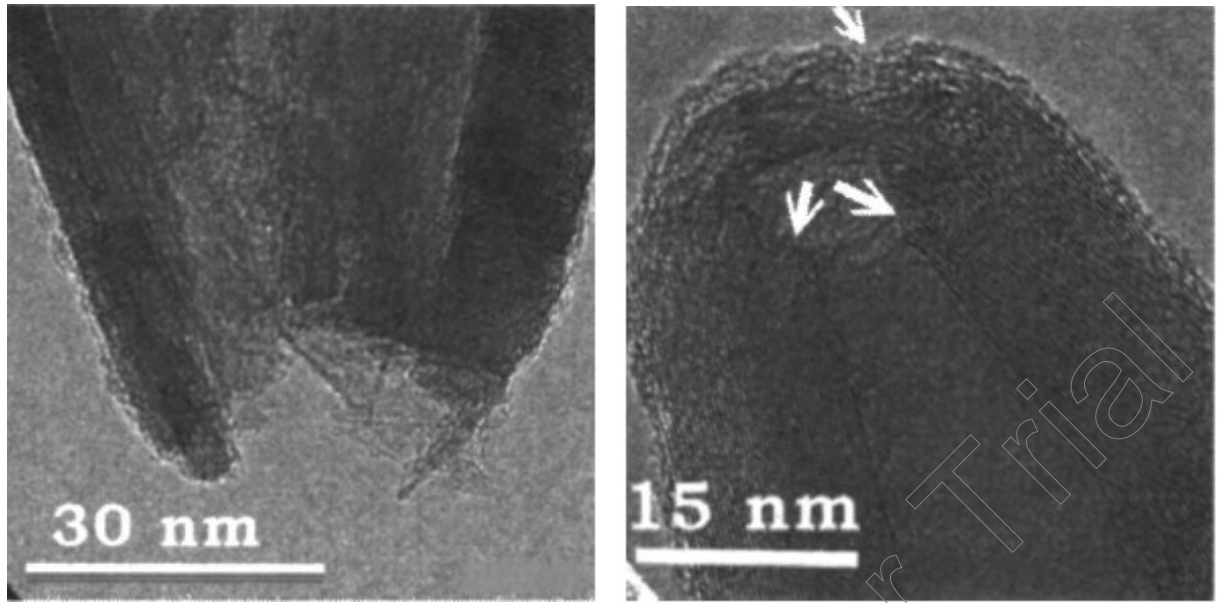
Fig. 2-5 TEM images of CNTs from a CNT array which was treated by O2 oxidation for 20 min at 400 °C [Kung 02-4819].
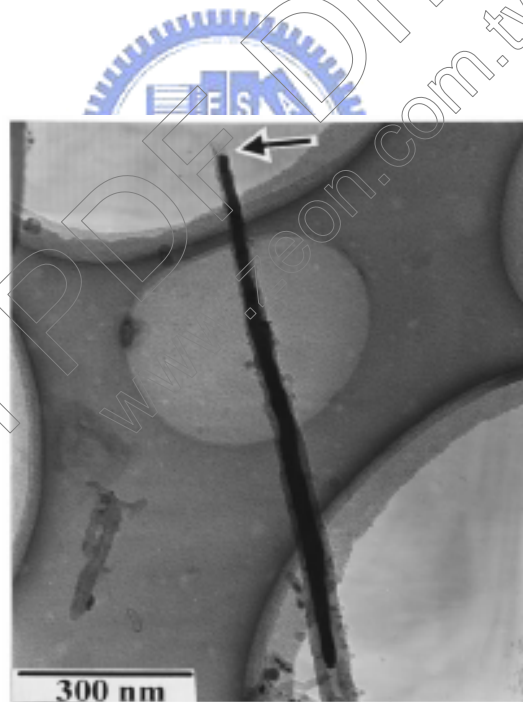


Fig. 2-6 TEM image, the molten Pd particles were drawn into the opened-tips and elongate to form Pd nanorods [Tsai 99-3462].
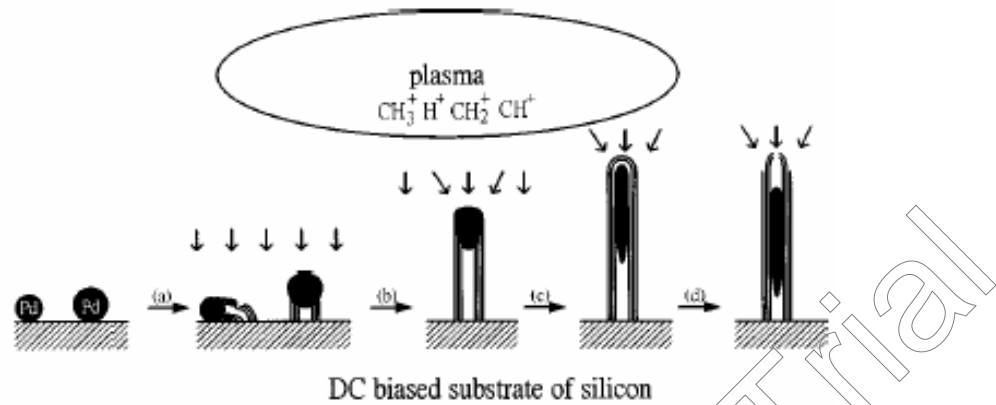
Figs. 2-7 Schematic of the growth mechanism, (a) nucleation of carbon nanotubes, (b) growth of carbon nanotubes and melting of the Pd nanoparticles,(c) sinking and elongating of the Pd droplet, and (d) opening of the carbon nanotubes and formation of the Pd nanorod. [Tsai 99-3462].
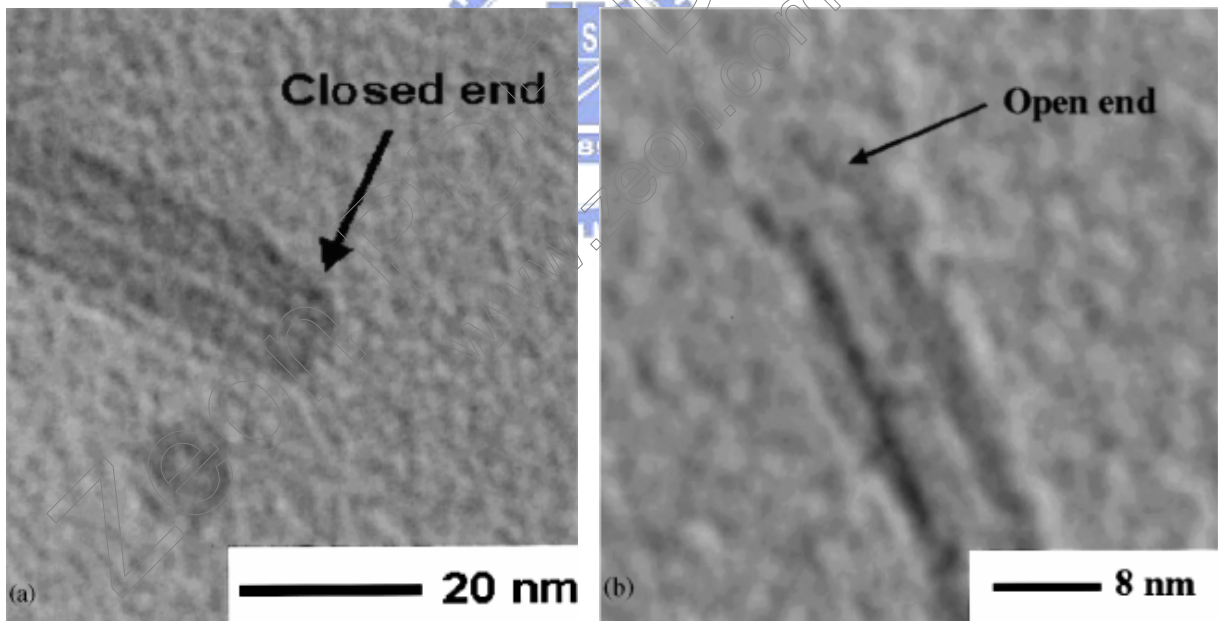


Figs. 2-8 A comparison of TEM bright-field image between conventional and a layer-by-layer deposited CNTs; (a) conventional CNTs (b) end point. [Chung 01-73]
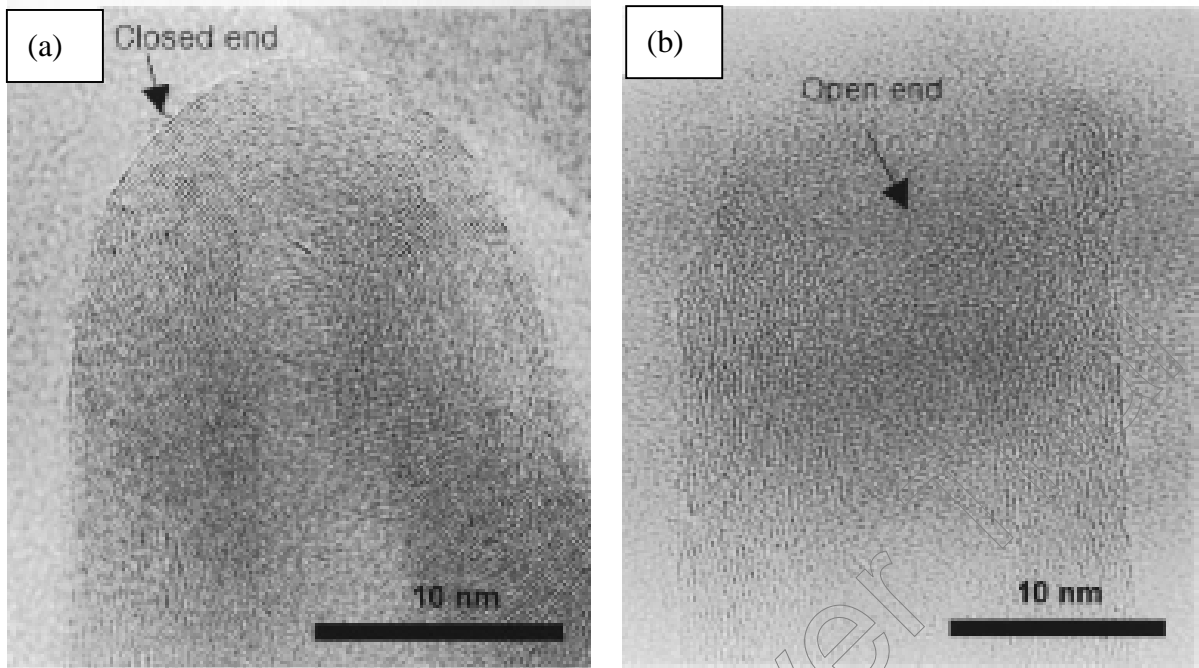
Figs. 2-9 Transmission electron microscopy images of (a) the curly and closed MWNTs grown in CH$_4$ and H$_2$ plasma by the PECVD method, (b) the aligned and open MWNTs grown using CH$_4$, H$_2$, and O$_2$ reaction gas [Lee 02-577].
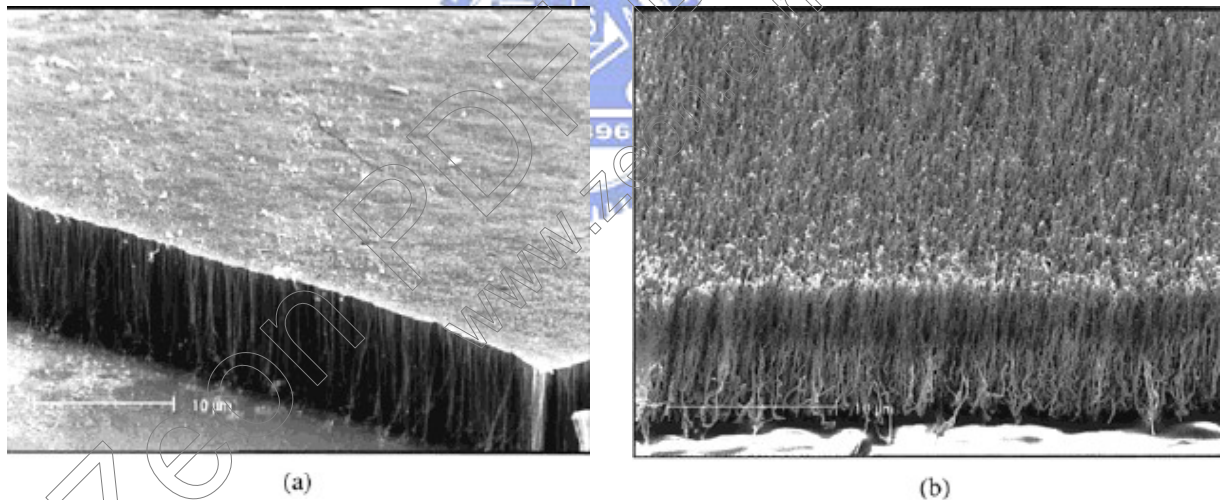


Figs. 2-10 SEM images of an aligned nanotube film before and after H$_2$O-plasma etching (a) a large area aligned nanotube film covered by a thin amorphous carbon layer on a quartz glass plate before plasma treatment, (b) the same nanotube film as (a) after the H$_2$O-plasma etching for 30 min at 250 kHz, 30 W, and 0.62 Torr. Note that the micrographs shown in (a) and (b) were not taken from the same spot due to technical difficulties [Huang 02-3543].
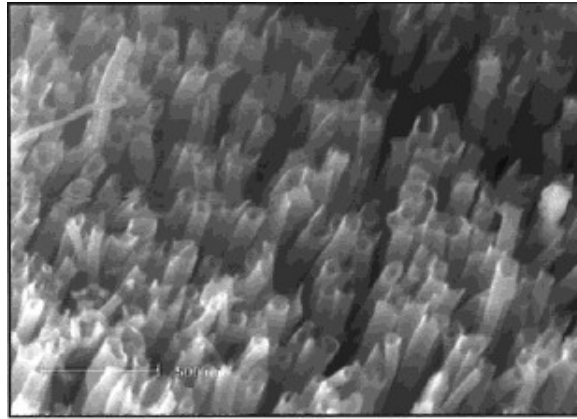
Fig.2-11 SEM images of the aligned nanotubes after the plasma-treatment for 80 min, followed by a gentle wash with HCl (37%) to remove the Fe catalyst residues [Huang 02-3543].
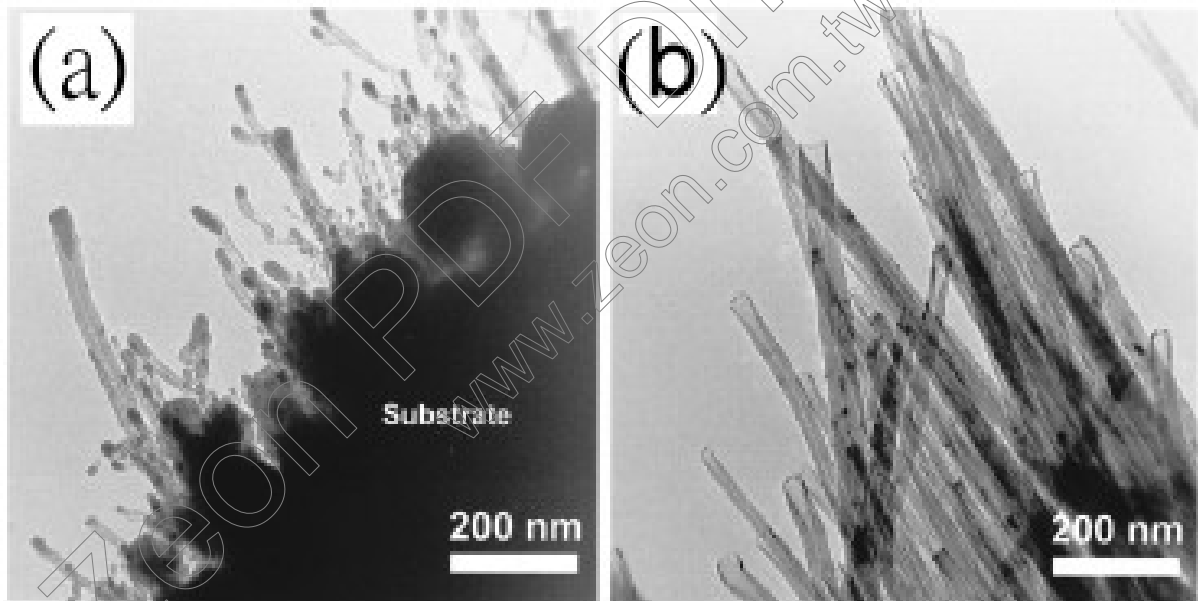


Figs. 2-12 TEM images(c) NTs with different diameters initially grown on the steel surface.

(d) Open-end NTs produced by electrochemical etching [Wang 01-4028].
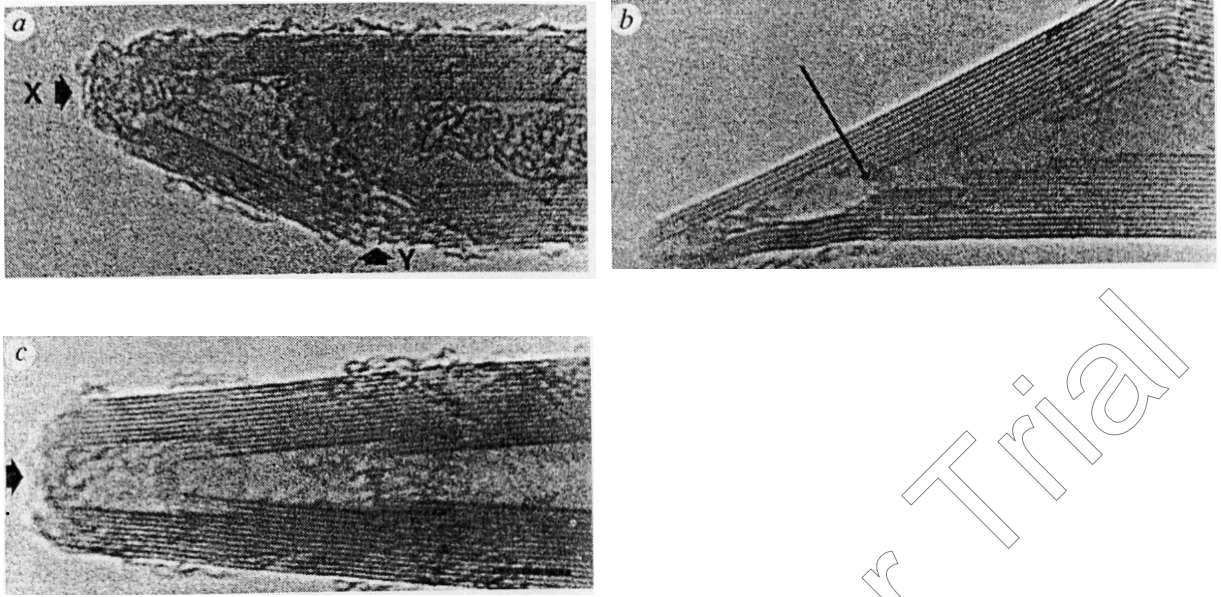
Figs. 2-13 Typical high-resolution electron micrographs of nitric acid treated nanotubes. (a) Attack has occurred at point X and Y where non-six-membered Carson ring are represent. (b) and (c), Arrows show site of the destruction of multiple internal caps by nitrite acid treatment. Scale bar, 50Å [Tsang 94-159].
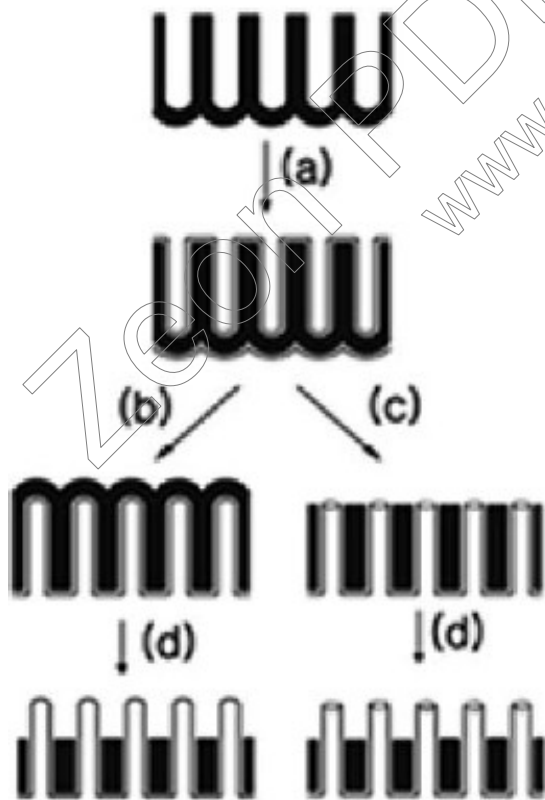


Figs. 2-14 Schematics of fabrication of the open and closed tip CNTs using AAO templates. The processes correspond to (a) fabrication of CNTs, (b) and (c) ion millings, and (d) etching in acid solution [Yoon 04-825].
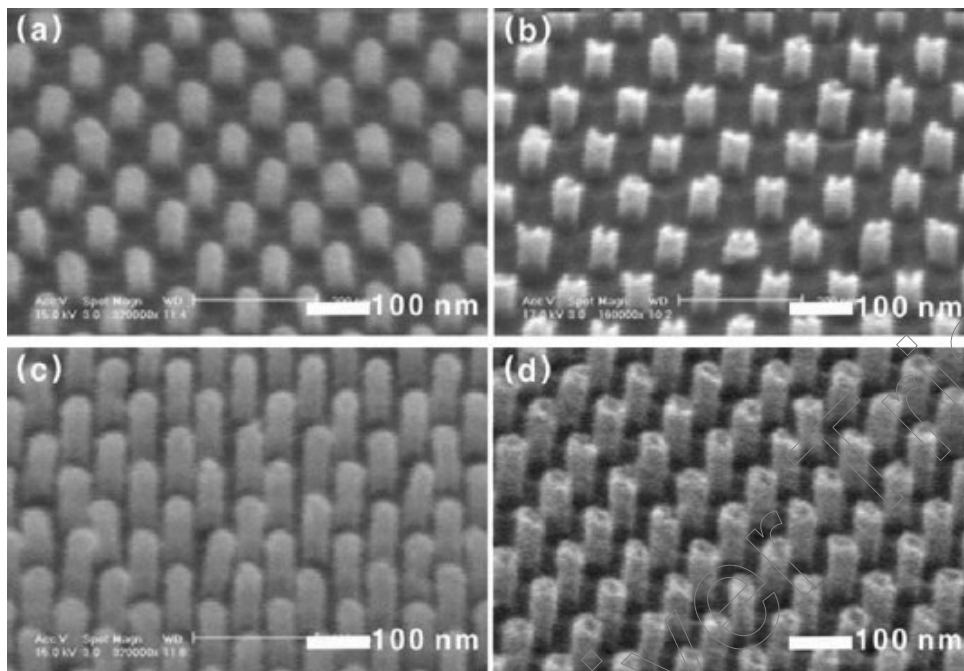
Figs. 2-15 SEM images of the closed (a), (c) and open (b), (d) tips of CNTs fabricated on AAO templates. The height of the tips could be controlled by changing the etching time in acid solution and its deviation was about ± 2 nm [Yoon 04-825].
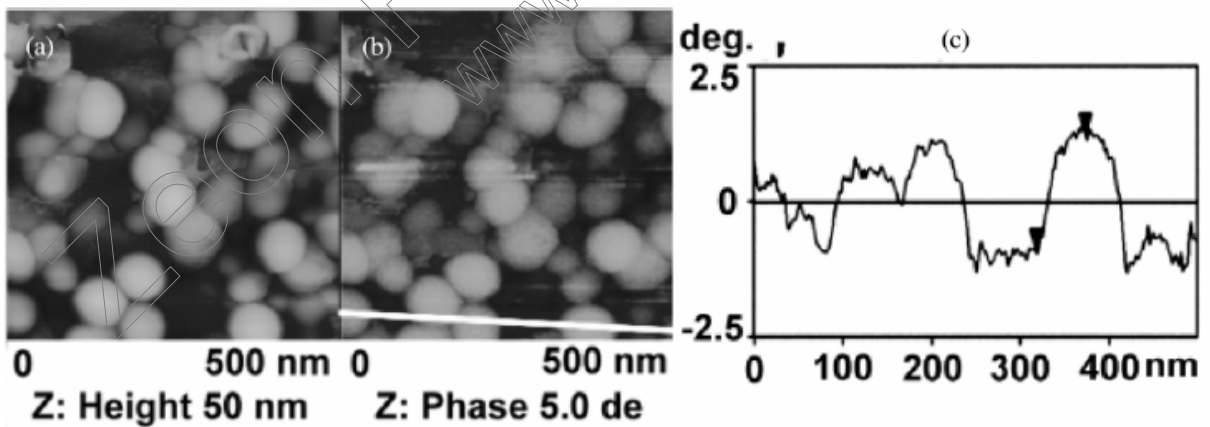


Figs. 2-16 (a) AFM image, (b) MFM image and (c) the corresponding MFM line scan profile for Fe catalyst-assisted CNTs, respectively [Kuo 03-799].
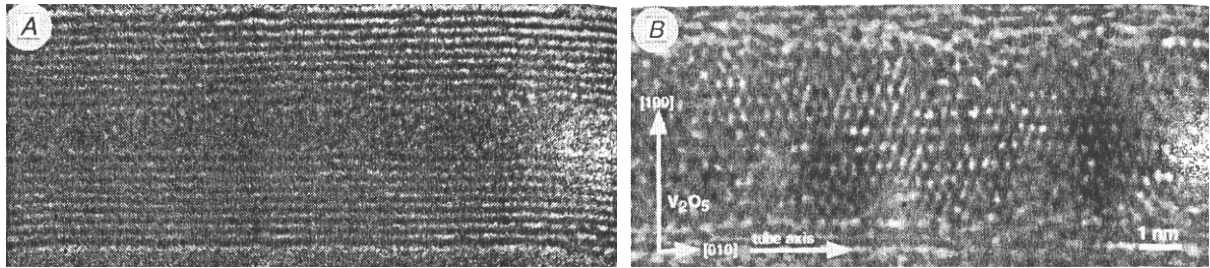
Figs. 2-17 High-resolution TEM images of tubes filled (darker contrast in the centre) with vanadium oxide. (a) Filling in a narrow internal hollow, showing amorphous structure. (b) Crystalline $V_2O_5$ structure in a larger hallow (only 2~3 tube layers around the filling is shown) showing preferred orientation with respect to the tube axis [Ajayan 95-564].
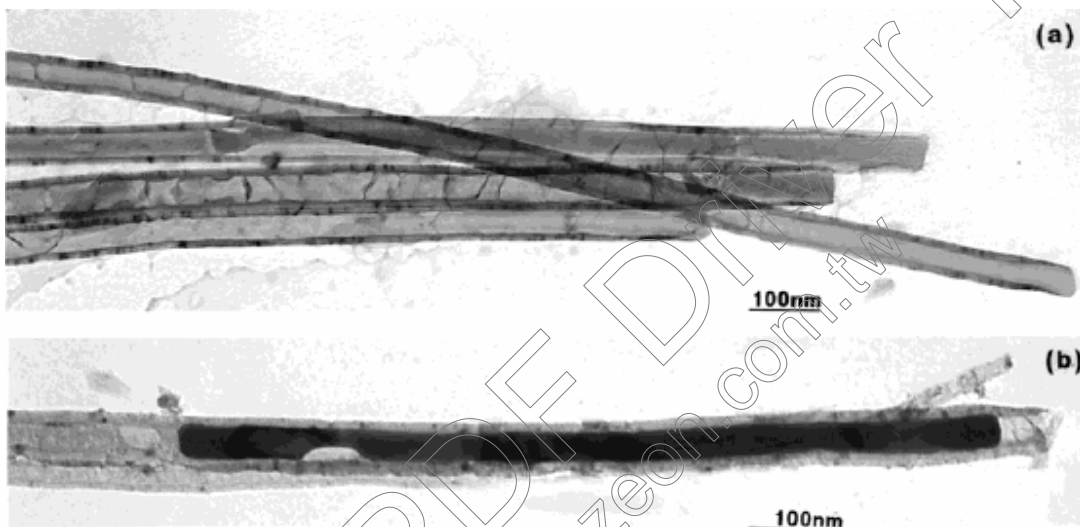


Figs. 2-18 TEM images of the opened carbon nanotubes (a) before and (b) after filling with the Ag nanorod. Note that the micrographs shown in (a) and (b) were not taken from the same nanotubes due to technical difficulties [Huang 02-3543].
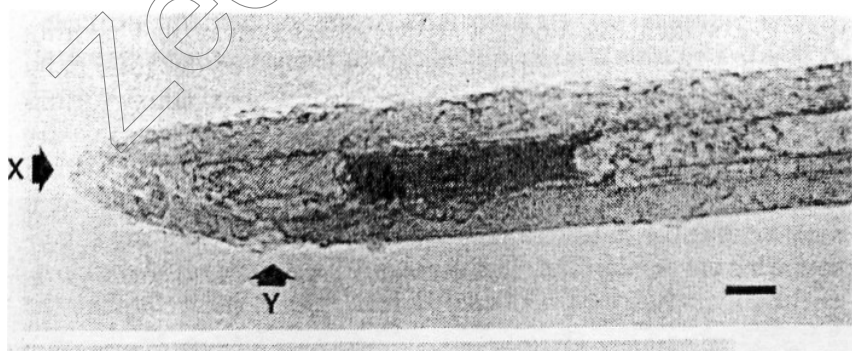


Fig. 2-19 High resolution electron micrograph of a nickel material filled nanotubes also opened at point X and Y; the observed fringes of $2.40 \pm 0.05$ Å correspond to (111) NiO crystal plane. Scale bar, 50 Å [Tsang 94-159].
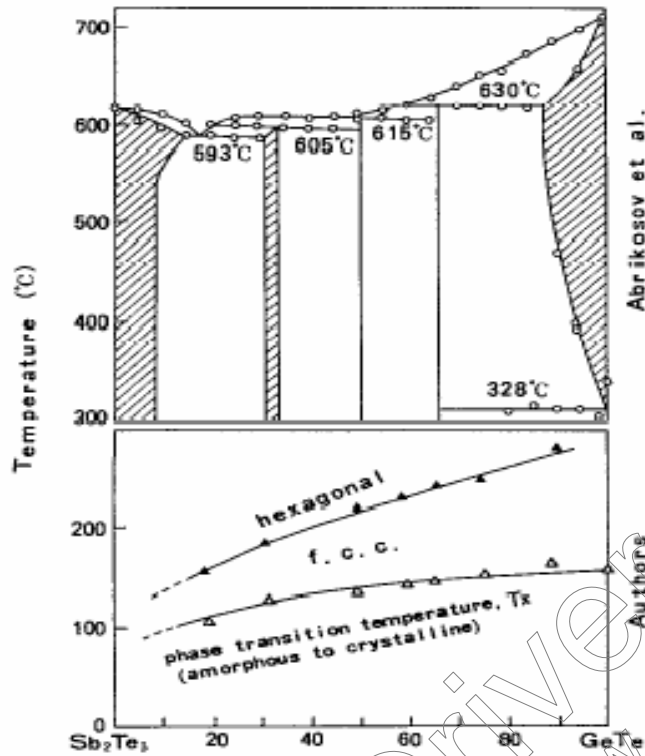
Fig. 2-20 GeTe-Sb$_2$Te$_3$ pseudobinary phase diagram and phase transition temperatures of GeTe-Sb, Te, pseudobinary amorphous alloy films [Yamada 91-2849].
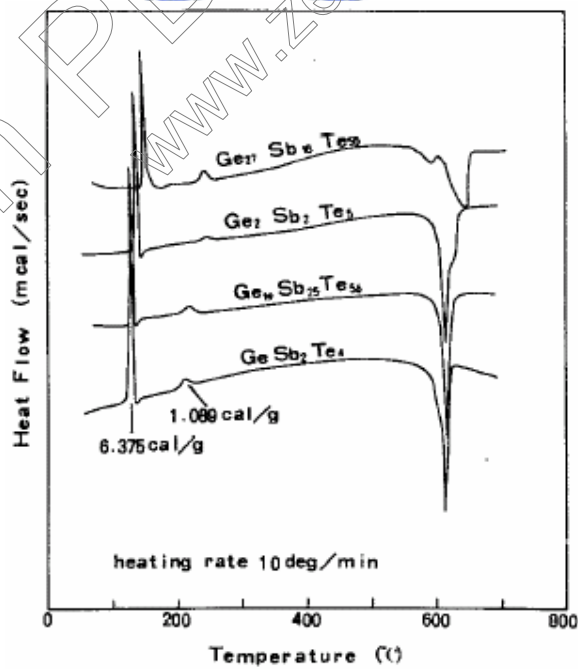


Fig. 2-21 DSC curves for the GeTe-Sb$_2$Te$_3$ psedobinary system at heating rate of 10 deg/min [Yamada 91-2849].